Journal of Applied Fluid Mechanics, Vol. 16, No. 10, pp. 2030-2040, 2023.
Available online at www.jafmonline.net, ISSN 1735-3572, EISSN 1735-3645.
https://doi.org/10.47176/jafm.16.10.1851

Energy Losses Assessment of Smallholder Farmers' Surface Water Irrigation Pumps in South and Southeast Asia Using Entropy Generation Principle

W. Sanghirun[1,3] and W. Asvapoositkul[2†]

[1] *The Joint Graduate School of Energy and Environment, King Mongkut's University of Technology Thonburi, Bang Mod, Thung Khru, 10140, Thailand*
[2] *Department of Mechanical Engineering, Faculty of Engineering, King Mongkut's University of Technology Thonburi, Bang Mod, Thung Khru, 10140, Thailand*
[3] *Center of Excellence on Energy Technology and Environment (CEE), Ministry of Higher Education, Science, Research and Innovation (MHESI), Thung Phayathai, Ratchathewi, 10400, Thailand*

†*Corresponding Author Email: wanchai.asv@kmutt.ac.th*

ABSTRACT

One of the most serious problems among smallholder farmers in South and Southeast Asia associated with the use of a surface water irrigation pump is low engine performance. The main cause of this low performance is the decrease in the flow field energy conversion mechanism caused by irreversible processes. The energy conversion theory suggests that pump efficiency is maximum when the loss is minimum. Whatever the origin of the losses, the deterioration in engine performance is due to a deterioration in the reversibility of the pump system. In this study, the pump is classified as the propeller impeller (PI), the improved axial or typical impeller (TI), and the conical hollow-shaped impeller (CI). Entropy production is applied to the pump on design improvement and loss sources location and mechanisms. The entropy production consists of viscous dissipation and turbulent dissipation. In this study, the pump design improvement of various designs based on entropy production has been studied in detail to predict energy loss in areas such as the inlet section, impeller, or discharge pipe. With the entropy generation, the optimum efficiency of different pump designs CI, PI, and TI were determined. The results showed that in all designs, more than 63% of the total entropy generation came from turbulent distribution. The flow in the pumps was analyzed in detail in comparison with entropy generation. It was found that the entropy generation rate increased in the secondary flow direction and was consistent with free-stream velocity. The PI design at the inlet pipe should be modified for reducing flow separation and entropy generation. All design impellers showed high energy losses, especially near the hub and tip along the leading edge and trailing edge. Therefore, it is possible to determine which features of the flow and entropy generation are relevant to the pump improvement.

Article History

Received February 28, 2023
Revised May 16, 2023
Accepted June 17, 2023
Available online July 29, 2023

Keywords:

Entropy generation
Surface water irrigation pump
CFD
Propeller impeller
Axial impeller
Conical hollow-shaped impeller

1. INTRODUCTION

Pumps have become necessary for surface water irrigation in regions of South and Southeast Asia area (Barker & Molle, 2004). They are used to access rivers, as well as canal and drain water, to provide flexibility in the reliability and delivery of surface water. This is done with an axial low-lift pump. It is comprised of a long tube through which a rotating shaft moves. The impeller is attached to the suction side of the shaft, while an engine propels the opposite end of the shaft. The design may not be in accordance with the standards of industrialized countries. Comprehensive measurements of the design and characteristics of surface water irrigation pumps in South and Southeast Asia can be seen in Sanghirun and Asvapoositkul (2022). Most of the surface water irrigation pumps in Thailand are manufactured by local companies and intended for domestic use, without any restrictions on the hydraulic design. The pump's main characteristics are a simple design with mobile operation, reliability,

Nomenclature

k	turbulence kinetic energy	T	temperature
q	heat flux	V	volume of fluid domain
s	specific entropy	ε	turbulent dissipation rate
$\bar{s}$	specific entropy due to the time-averaged	ρ	density of fluid
$\acute{s}$	specific entropy due to turbulent fluctuation	μ	viscosity of fluid
$\dot{s}_{\bar{D}}'''$	entropy generation rate by viscous dissipation	Φ	viscous dissipation of mechanical energy
$\dot{s}_{\acute{D}}'''$	entropy generation rate by turbulent dissipation	Φ_θ	dissipation by heat transfer with temperature gradients
$\dot{s}_D$	the total entropy generation rate	ω	turbulence eddy frequency

durability, and relatively cheap. This has been proven for more than 50 years since it was invented and more recently in the Thai cave rescues (The Tham Luang cave rescue : A Global Mission, 2018). However, it has low efficiency. The optimal design parameters of this irrigation pump were successfully demonstrated by Yu and Colton (2017). The numerical simulation results reveal that the pump efficiency may be increased from 40.2% to 54.2% when operated at 1500 rpm. These are in the range of this current design parameters. Further improvement is possible by using analytical and CFD approaches, especially for performance improvement by an appropriate combination of operating conditions and geometry design. In this way, the relationship between the internal flow and the pump design could be analyzed for design development. This paper improves the current design of Thai irrigation pumps as smallholder famers' irrigation pumps in the regions of South and Southeast Asia by applying the entropy production principle to find the regions involved in losses. Consequently, numerical models (using analytical and/or CFD approaches) can improve the current design of the pumps efficiently.

The entropy generation method aims to use available energy resources in the most effective way (Sciacovelli et al., 2015). This cannot be achieved with the traditional energy balance approach alone. It is used to estimate the hydraulic loss distribution in hydraulic machineries, like secondary vertices, backflow, rotating stall, etc. An issue with this is the difficulty in calculating entropy generation. It can be used to determine working conditions or geometric parameter designs that will be compared to arrive at minimum levels of entropy generation. Therefore, entropy generation is an ideal design tool for the irreversibility minimization technique.

2. ENTROPY PRODUCTION METHODS APPLICATION

Irreversible energy loss caused by heat transfer and fluid viscosity is the main loss in turbomachines. The irreversibility can be quantitative as entropy production. In general, entropy production depends on viscous effects and heat transfer (Denton, 1993). The calculation method for entropy production in turbulent shear flows was developed by Kock and Herwig, 2004, 2005 and subsequently integrated into the CFD code. The method of entropy generation has been utilized in numerous engineering equipment such as centrifugal pumps, axial flow pumps, and turbines.

Hongyu et al. (2021) studied the influence of the angle between the guide vane trailing edge and the volute tongue on the hydraulic performance of a centrifugal pump by applying entropy generation. The result showed that the entropy production is minimum at the maximum efficiency with an angle of 50°. The energy loss in the centrifugal pump was mainly due to turbulent and wall friction dissipation (Huang et al., 2021). The mixed-flow pump's blade thickness effect on hydraulic losses was studied by Ji et al. (2021) using the entropy production method. The result showed that backflow vortex, secondary flow, and stall vortex were the major losses. The energy loss based on entropy production in the vertical axial flow pump was investigated by Yang et al. (2022). The impeller was the largest loss with more than 40%. The main entropy generation in the pump was dominated by turbulent dissipation and contributed up to 77% of the total entropy generation. The energy loss in terms of entropy production in hydro turbines was reported by Gong et al. (2013). The results showed that the runner of the turbine was the main loss with nearly 55%. Most of the entropy production was at the leading edge and the trailing edge of the runner where the shock and flow separation occurred. The entropy production in the pump turbine was examined by Li et al. (2016). The main energy loss was attributed to phenomena such as backflow and flow separation occurring within the runner, guide vanes, and stay vanes. Pei et al. (2016) studied the entropy production in a turbine and found that the maximum entropy production was at the leading edge of the impeller. The entropy production caused by turbulence dissipation was higher than that of viscous dissipation. The energy loss based on entropy production in the Francis turbine was investigated by Yu et al. (2022). The highest loss was in the draft tube where viscous dissipation was dominated.

From the research above, in turbomachinery, the entropy generation method is a widely accepted method for determining energy loss, which can be applied to improve the design of these devices for optimum efficiency. Nevertheless, the application of the entropy generation method has not been found to assess the energy loss of surface water irrigation pumps in the regions of South and Southeast Asia. In this study, the pump design improvement of various designs based on entropy

production is used to predict energy loss in tandem with the traditional energy balance method.

In CFD, the governing equations based on mass, momentum, and energy principles are solved to produce the expected physical fluid flow properties, such as velocity, pressure, and temperature. These flow field properties can be used to determine entropy since entropy depends on pressure and temperature. The entropy is created due to the effects of viscous and heat transfer. The entropy generation for single-phase incompressible flow can evaluate by the following (Spurk, 1989).

$$\frac{\partial}{\partial t}(\rho\, \nabla.s) = -\nabla.\left(\frac{q}{T}\right) + \frac{\Phi}{T} + \frac{\Phi_\Theta}{T^2} \tag{1}$$

where s is specific entropy, q is heat flux, Φ is viscous dissipation of mechanical energy and Φ_Θ is dissipation by heat transfer with temperature gradients (Kock & Herwig, 2004).

Based on the Reynolds Averaged Navier Stokes (RANS) approach, all the flow properties for turbulent flow are expressed as mean and fluctuation values. For example, s = $\bar{s} + \acute{s}$, where the bar superscript represents the mean value and the prime superscript represents the variation because of turbulent fluctuation.

The equation for incompressible turbulent flow is

$$\frac{\partial}{\partial t}(\rho\, \nabla.(\bar{s} + \acute{s})) = -\nabla.\left(\frac{q}{T}\right) + \frac{\bar{\Phi}}{T} + \frac{\overline{\Phi_\Theta}}{T^2} \tag{2}$$

where $\frac{\bar{\Phi}}{T}$ is the entropy production due to viscous dissipation and $\frac{\overline{\Phi_\Theta}}{T^2}$ is the entropy production due to heat transfer.

In an isothermal steady-state flow condition, entropy production is a function of viscous dissipation only. The viscous dissipation, in the calculation of time-averaged entropy production for turbulent flow, consists of dissipation in the mean flow field (or viscous dissipation) and dissipation in the turbulent fluctuations of the velocity (or turbulent dissipation).

$$\frac{\bar{\Phi}}{T} = \dot{s}_{\bar{D}}''' + \dot{s}_{\acute{D}}''' \tag{3}$$

The two entropy terms are simplified to

$$\dot{s}_{\bar{D}}''' = \frac{\mu}{T}\left\{2\left[\left(\frac{\partial \bar{u}}{\partial x}\right)^2 + \left(\frac{\partial \bar{v}}{\partial y}\right)^2 + \left(\frac{\partial \bar{w}}{\partial z}\right)^2\right] + \left(\frac{\partial \bar{u}}{\partial y} + \frac{\partial \bar{v}}{\partial x}\right)^2 + \left(\frac{\partial \bar{u}}{\partial z} + \frac{\partial \bar{w}}{\partial x}\right)^2 + \left(\frac{\partial \bar{v}}{\partial z} + \frac{\partial \bar{w}}{\partial y}\right)^2\right\} \tag{4}$$

$$\dot{s}_{\acute{D}}''' = \frac{\mu}{T}\left\{2\left[\overline{\left(\frac{\partial u'}{\partial x}\right)^2} + \overline{\left(\frac{\partial v'}{\partial y}\right)^2} + \overline{\left(\frac{\partial w'}{\partial z}\right)^2}\right] + \overline{\left(\frac{\partial u'}{\partial y} + \frac{\partial v'}{\partial x}\right)^2} + \overline{\left(\frac{\partial u'}{\partial z} + \frac{\partial w'}{\partial x}\right)^2} + \overline{\left(\frac{\partial v'}{\partial z} + \frac{\partial w'}{\partial y}\right)^2}\right\} \tag{5}$$

where μ is viscosity of fluid and u, v and w are the velocities in the x, y, and z directions.

The rate of local entropy production via viscous dissipation ($\dot{s}_{\bar{D}}'''$) is evaluated through the velocity gradient and temperature from the CFD result. However, the rate of local entropy production via turbulent dissipation ($\dot{s}_{\acute{D}}'''$) cannot be calculated similarly, because the fluctuating velocity component is not obtained from the CFD result (Launder & Spalding, 1974). It can be related to the turbulence model as follows (Herwig & Kock, 2007).

In k-ε turbulent model, the rate of local entropy production via turbulent dissipation is evaluated by

$$\dot{s}_{\acute{D}}''' = \frac{\rho.\varepsilon}{T} \tag{6}$$

where ρ, ε, and T stand for density, turbulent dissipation rate and temperature, respectively.

In k-ω turbulent model, the rate of local entropy production via turbulent dissipation is evaluated by

$$\dot{s}_{\acute{D}}''' = \beta\frac{\rho\omega k}{T} \tag{7}$$

where β represents a constant of 0.09 (Mathieu & Scott, 2000), ω represents turbulence eddy frequency and k represents the turbulence kinetic energy.

Therefore, the rate of total entropy production in the flow field volume ($\dot{s}_D$) is evaluated as follows.

$$\dot{s}_D = \int_v \dot{s}_{\bar{D}}'''\, dV + \int_v \dot{s}_{\acute{D}}'''\, dV \tag{8}$$

where V represents the fluid domain volume.

3. METHODOLOGY AND CFD SETUP

Three designs of Thai irrigation pump impellers denoted by the propeller (PI), the improved axial or typical impeller (TI), and the conical hollow-shaped impeller (CI) were investigated. The PI and TI are manufactured and sold by local factories. The CI is designed by (Asvapoositkul & Sanghirun, 2023; Sanghirun & Asvapoositkul, 2019, 2020a, b). Figure 1 and Table 1 show the design and geometric parameters.

The original design of PI was basically a boat propeller for pumping large volumes at low heads and non-clogging performance (Chinsuwan & Cochran, 1986; Natural Resources Conservation Service, 2016). The propeller impeller diameter is 230 mm with 5 blades (see Fig. 1(a)). Figure 1(b) shows the TI design which is the modified version of PI and is popular in South and Southeast Asia (Chinsuwan & Cochran, 1985; Yu & Colton, 2017). This impeller has 6 blades made of mild steel. The inlet portion of the pump is enlarged.

The CI impeller, see Fig. 1(c), diameter is 139 mm with 4 blades. The comparative performance of designs PI and TI was carried out at 1,000 rpm, and of design CI was carried out at 1,400 rpm. The pumps were performed at different speeds due to the recommendation from the manufacturers and their design conditions. Maximum efficiency values of test designs PI, TI, and CI were in the range of 35 – 55%, respectively at each design flow rate (Sanghirun & Asvapoositkul, 2022). The experimental results also show that the PI and TI designs operate with steep pump curves. The CI design operates with flat pump curves. This means that the PI and TI pump working conditions are more variations to flow changes than that of the CI pump. In practice, irrigation pumps are often not operated near their best efficiency point, causing major energy losses. The changes in consumption and/or

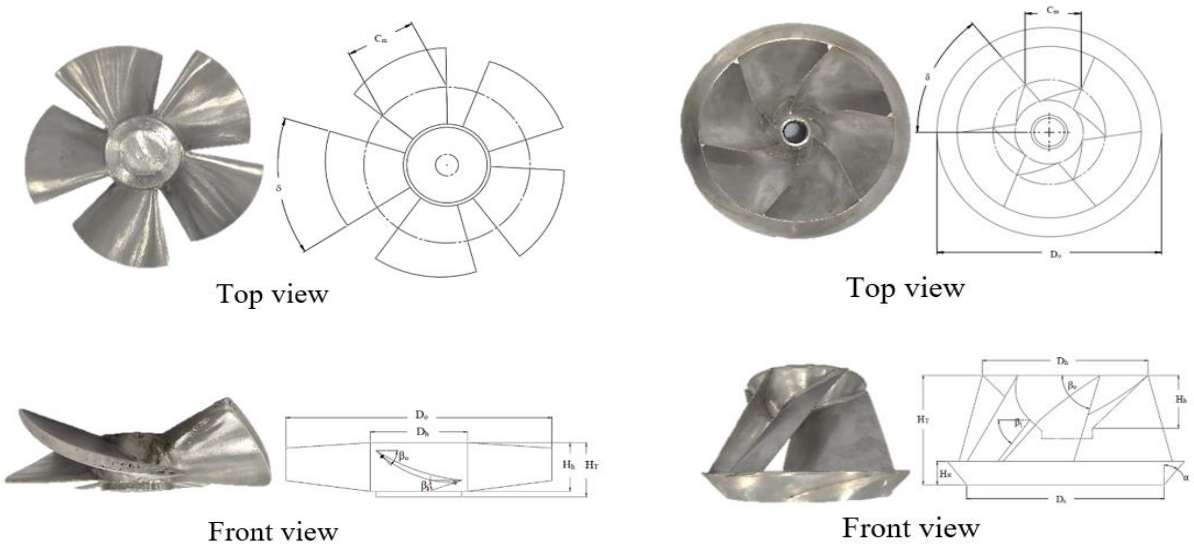

(a) PI impeller (b) TI impeller

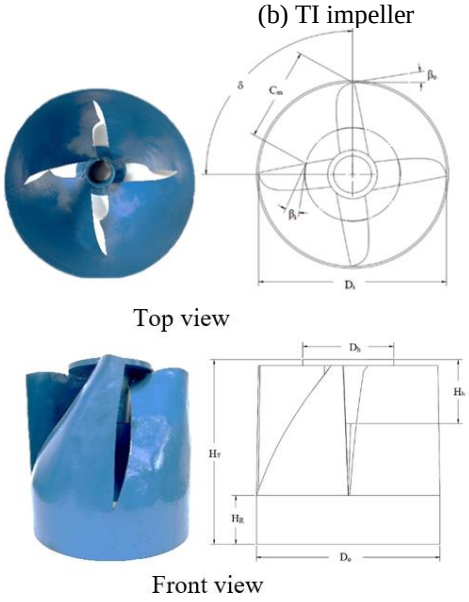

(c) CI impeller

Fig. 1 Basic parameters for design of Thai irrigation pump impellers PI, TI, and CI

pressure are common due to the season. Accordingly, a flat efficiency curve would be more desirable for this kind of pump. Each pump performance curve can be seen in Sanghirun and Asvapoositkul (2022). Pump heads, Powers, and efficiency of each design at BEP are shown in Table 2 for comparison.

Computational fluid dynamics (CFD) is applied to study on design of PI, TI, and CI. CFD solutions provide all information to calculate the rate of entropy production. In this way, the physical flow and loss production via viscosity in the pumps can be compared and investigated. Then the predicted result is evaluated to improve the machine's performance by adjusting its design parameters.

The computational domain consists of three sub-domains (extended inlet section including the inlet mouth, the impeller, and the outlet pipe) as presented in Fig. 2. The simulated pump domain had an inlet domain height extended to 2 × D to account for turbulent boundary conditions before the flow reached the inlet boundary. The pump head is determined by the total pressure differential between the inlet and outlet boundaries. Each sub-domain is connected by domain interfaces to complete the entire domain. The impeller employs a rotating frame of reference, while the rests employ a stationary frame of reference.

A frozen frame of reference is applied in relative positions between the impeller and the inlet, and the outlet pipes. In this study, the Shear Stress Transport (SST) model was used to accurately resolve the fluid flow problem. This model works by treating the model based on turbulence/frequency (k-ω) at the wall and k-ε in the bulk flow (Ansys, 2018; Mathieu & Scott, 2000).

Dense cell layers were set close to walls since most losses, flow separation, and vortices occur near those areas. Clustered grids near wall surfaces were also applied to effectively capture viscous effects. The mesh

Table 1 Design parameters of each design

Parameter	Description (unit)	PI	TI	CI
Z	Number of blades (-)	5	6	4
D_o	Outside diameter of impeller (mm)	230	240	139
D_i	Inside diameter of impeller (mm)	-	190	136
D_h	Hub diameter of impeller (mm)	84	151	69
D_P	Diameter of pipe (mm)	242	253	149
D_{OP}	Outlet pipe diameter (mm)	200	200	149
H_T	Total height of impeller (mm)	52	142	140
H_h	Hub height (mm)	51	78	37
H_R	Inlet ring height (mm)	-	27	49
C_m	Chord length (mm)	67	87	76
δ	Volute angle (°)	57	52	90
α	Ring angle (°)	-	45	-
β_i	Inlet blade angle (°)	2	53	10
β_o	Outlet blade angle (°)	55	50	13
n	Impeller speed (rpm)	1,000	1,000	1,400
$\dot{\boldsymbol{Q}}$	Mass flow rate at BEP (kg/s)	55	55	40
H	Total head pump at BEP (m)	1.87	2.68	1.58
η	Pump efficiency at BEP (%)	34.66	46.49	54.77
-	Inlet mouth	×	✓	✓
-	Outlet guide vane	✓	✓	✓

Table 2 The results of the experimental and simulation of each design at BEP

Impeller design	Performance parameters								
	Total head pump at BEP			Power at BEP			Pump efficiency at BEP		
	H-Exp. (m)	*H-Sim.* (m)	Error (%)	P_s-*Exp.* (kW)	P_s -*Sim.* (kW)	Error (%)	η-*Exp.* (%)	η -*Sim.* (%)	Error (%)
PI	2.68	2.77	3.35	3.11	2.88	7.39	46.49	50.09	3.60
TI	1.87	1.96	4.81	2.65	2.45	7.54	34.66	39.12	4.46
CI	1.58	1.65	4.43	1.13	1.15	1.26	54.77	56.13	1.36

independence, as well as quality, were checked. The total computational domain size was about 8×10^6 elements with average y^+ values smaller than 10.

4. RESULTS

To validate the accuracy and reliability of the present prediction method, the comparative results with those reported by Sanghirun and Asvapoositkul (2022) are presented first. The results are presented in Table 2. The error from the predicted total head, input power, and pump efficiency at BEP of each design is less than 8%. These predictions and experimental results are strongly correlated, with entropy generation being the lowest at BEP. The most efficient pump is CI with the lowest total entropy generation rate, followed by TI and PI, respectively. In this study, entropy generation is applied to locate loss sources in various pump designs. Comparative results of the CFD are presented as velocity vector and entropy generation contours.

The entropy generation rates at the peak efficiency of PI, TI, and CI pump designs are shown in Fig. 3. It also indicates that more than 63% of all entropy generation is turbulent dissipation in all designs. The domination of turbulent dissipation in all designs indicates a high affecting of viscous forces on the fluid body. These turbulent velocity fluctuations lead to a breakdown of eddies. The entropy generation rate can be applied to the pump on design improvement and loss sources location and mechanisms. To complete this, each design and location are investigated in the followings.

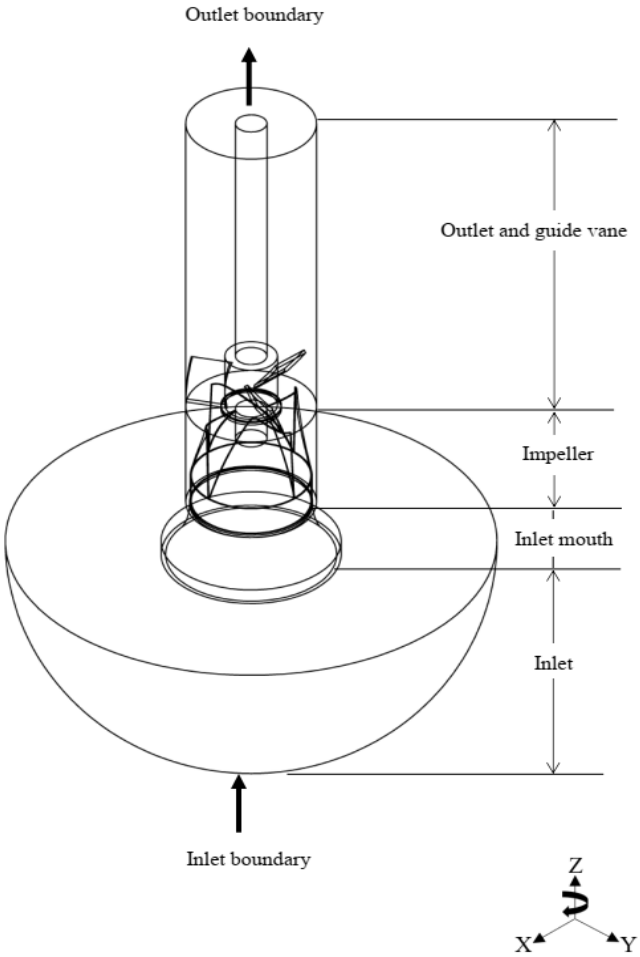

Fig. 2 Computational domain of Thai irrigation pump impellers PI, TI, and CI

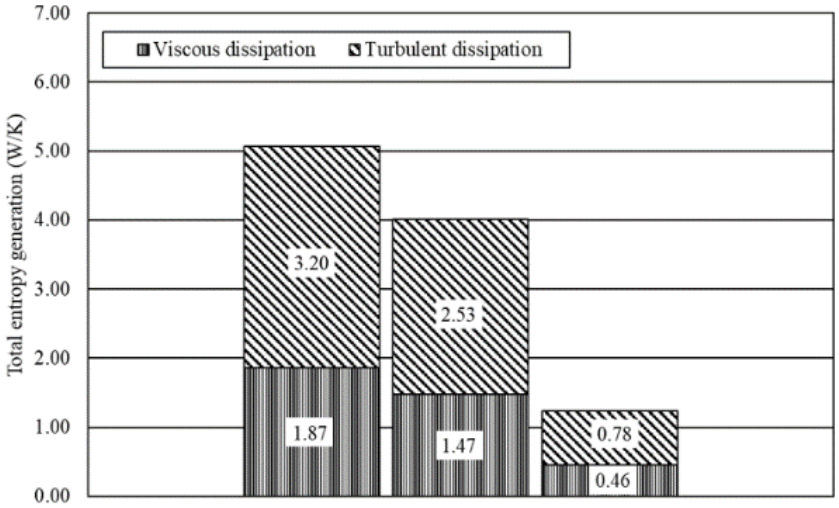

Impeller	PI	TI	CI
Viscous dissipation (%)	36.85	36.72	36.94
Turbulent dissipation (%)	63.15	63.28	63.06
Total entropy generation (W/K)	5.06	4.04	1.24

Fig. 3 Comparative effects of entropy generation on pump designs PI, TI and CI at BEP

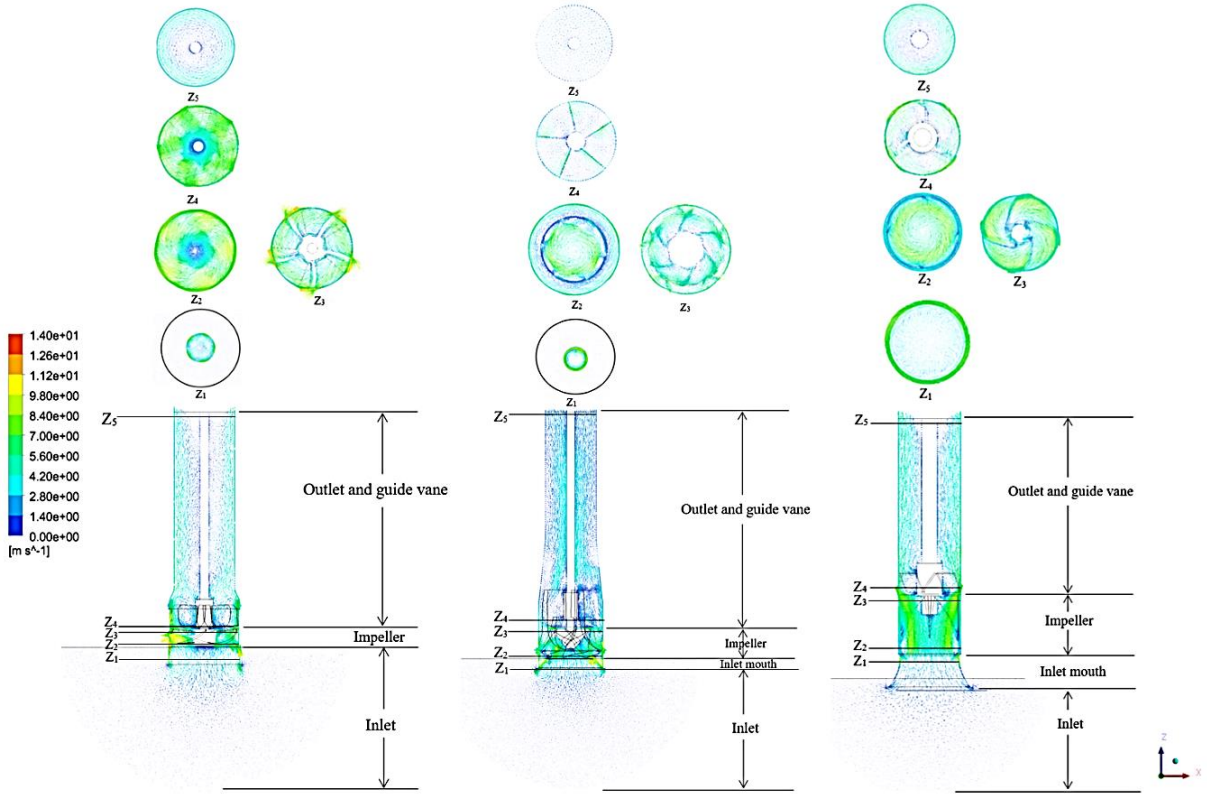

(a) PI (b) TI (c) CI

Fig. 4 Velocity vectors on the cross-sectional planes in designs PI, TI and CI

Figure 4 presents the velocity flow field in each design. The cross-section plane along the center line of the shaft as well as along the pipe height are shown for further investigation. In design PI, the separation zone in the portion of the blade is larger when compared to the designs TI and CI. Areas of high re-circulation values can be found in the inlet pipe, the blade surface, and the outlet guide vane. When comparing the three designs, we can infer that the CI, with an inlet mouth and outlet guide vane, leads to a less separated flow field.

Figure 5 shows entropy contours in the three designs at the same section planes as that in Fig. 4. At the inlet pipe, the production of entropy in PI is more intensive than that in the impeller and outlet guide vane.

On the other hand, in CI and TI more intensive entropy generation is in the impeller of each design. One can see in Fig. 4 and Fig. 5 that the large flow separation areas lie in the region of high entropy generation. Without an inlet mouth in PI, areas with high re-circulation, and high entropy generation at the rim of the inlet tube are larger than that in TI and CI with an inlet mouth. Large separation areas on blade surfaces may be caused by vortex flows due to higher incidence angles. This can be described by investigating the flow mechanism on the pump blade near both the suction surface and pressure surface.

The predicted velocity vectors adjacent to the blade surface of PI are presented in Fig. 6 with high magnitude due to high tip speed. In Fig. 6(a), the separation flow is at the leading edge near the hub and tip. The fluid is moving from the hub to the tip. The secondary flows near the pressure surface (Fig. 6(b)) are higher compared to those near the suction surface. This secondary flow will move fluid particles to the tip of the blade. The separation zone on the blade surface is high at the tip region. It is possible to compare the velocity flow field as well as entropy production on the blade surface of each design. Figure 7 shows the contours of entropy production on the blade surface of PI. Almost the whole area of the blade shows a high value of entropy generation. The intense entropy production on the blade surface, especially at the leading edge and at the tip, indicates high losses because of high flow. It contributes significantly to the entropy rise or overall pump loss.

The predicted velocity vectors adjacent to the suction surface of TI are presented in Fig. 8(a). The secondary flow is very strong from the leading edge. The fluid is moving from the hub and tip to the middle region. As shown in Fig. 8(b), the pressure surface presents similar results as those from the suction surface. In this case, the fluid is moving from the hub to the tip.

Figure 9 shows the contours of the predicted entropy production on the blade surface of TI. The entropy production is very high at the leading edge and the trailing edge of the blade. On the suction surface, the loss is high along the middle region of the blade. On the pressure surface, the loss is high along the upper region of the tip.

The predicted velocity vectors adjacent to the suction surface of CI are presented in Fig. 10(a). There is flow separation near the leading edge of the hub and the tip. The strong secondary flows are indicated from about the beginning of the axial-radial bend up to the trailing edge.

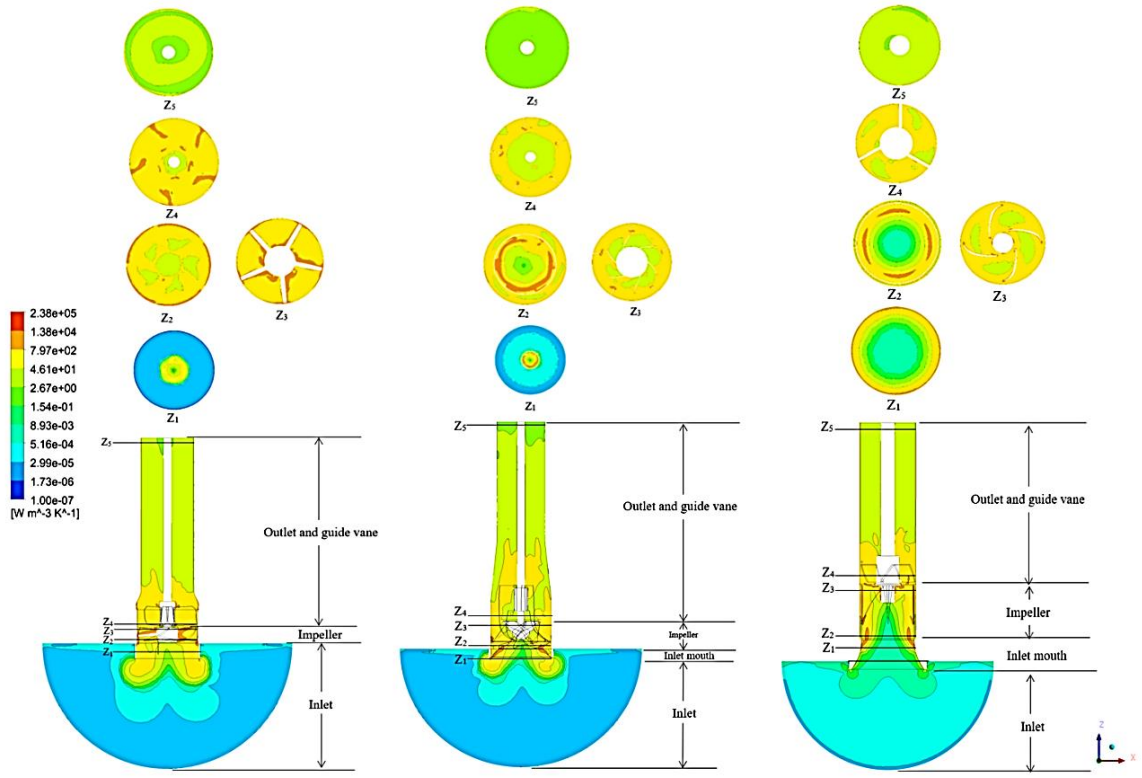

(a) PI (b) TI (c) CI

Fig. 5 Contours of total entropy generation on the cross-sectional planes in designs PI, TI and CI

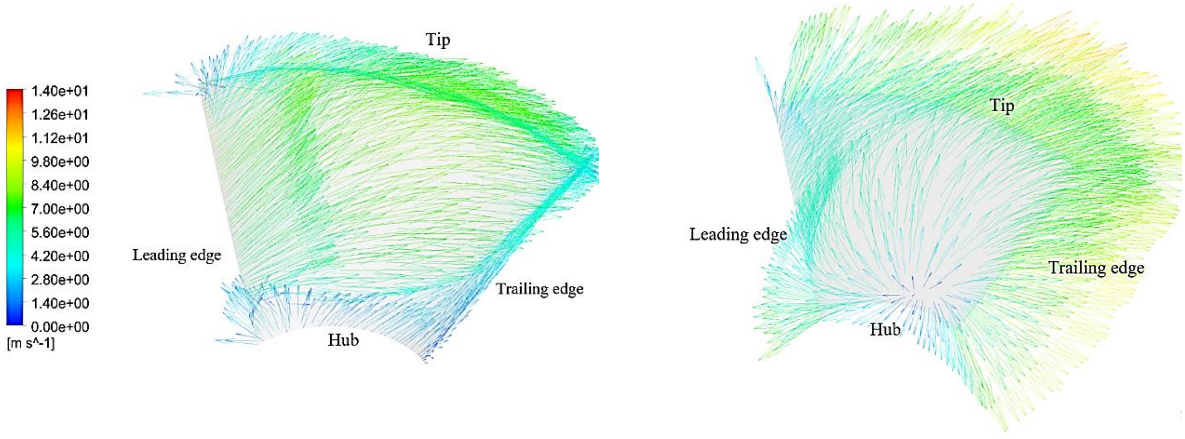

(a) Suction surface (b) Pressure surface

Fig. 6 Predicted velocity vectors near the blade surface of PI impeller

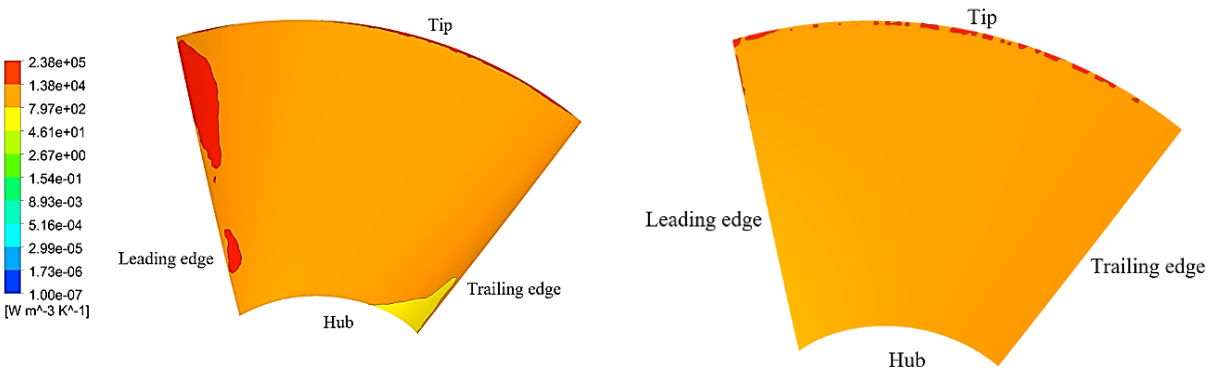

(a) Suction surface (b) Pressure surface

Fig. 7 Contours of total entropy generation on blade surface of PI impeller

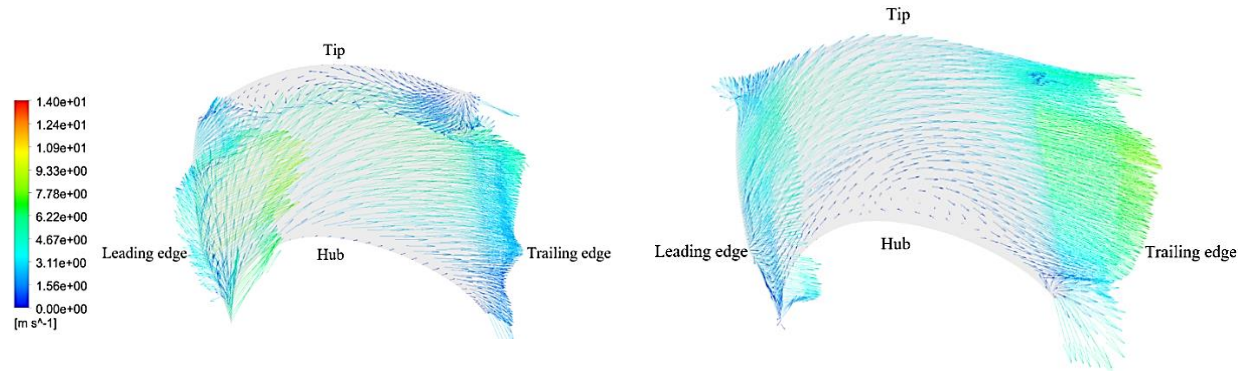

(a) Suction surface (b) Pressure surface

Fig. 8 Predicted velocity vectors near the blade surface of TI impeller

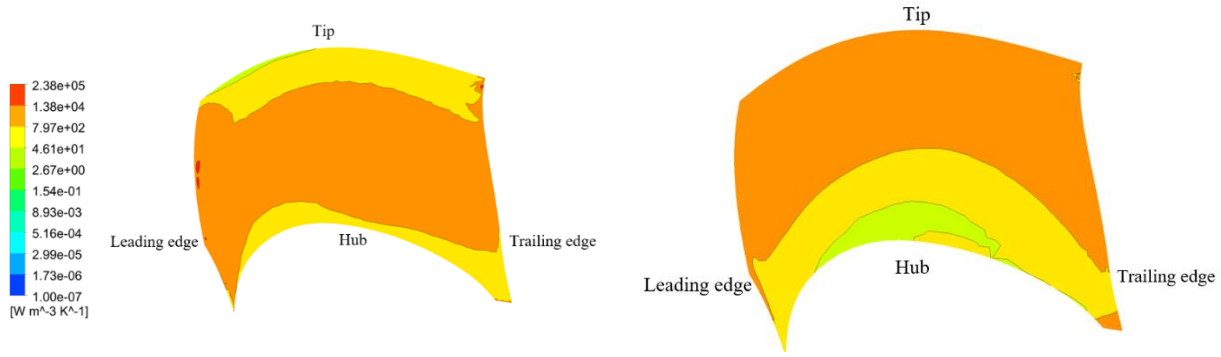

(a) Suction surface (b) Pressure surface

Fig. 9 Contours of total entropy generation on blade surface of TI impeller

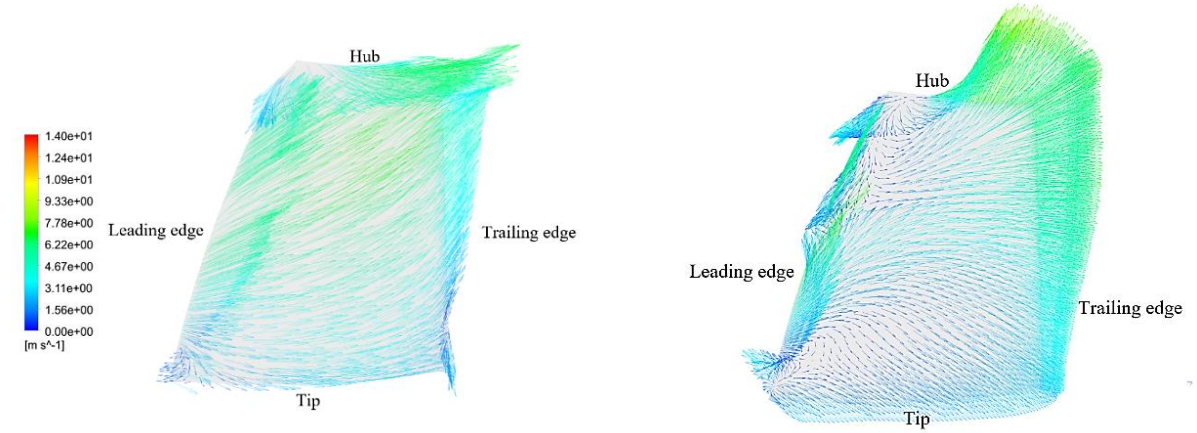

(a) Suction surface (b) Pressure surface

Fig. 10 Predicted velocity vectors near the blade surface of CI impeller

They grow significantly in the hub and tip. Therefore, fluid particles will move to the hub and tip of the blade. In Fig. 10(b), there is flow separation in the corner of the leading edge near the hub and tip of the pressure surface. From this figure, the strong secondary flow is indicated at about the middle of the leading edge where the flow separation forms. Therefore, the fluid is moving to those areas. The secondary flows present on the suction surface are greater in magnitude compared to those on the pressure surface (Fig. 10(a)) because of low-velocity magnitude. The secondary flows adjacent to the pressure surface at the leading edge are directed in the opposite direction of the other region. The main reason may be that the free-stream velocity is inconsistent with the angle of the blade at the leading edge.

Figure 11 shows entropy contours on the blade surface of CI. The loss is high at the blade's leading edge and, trailing edge, especially along the hub. We can see that there is flow separation in the hub region on the suction blade surface, as shown in Fig. 10. Secondary flow occurs in areas adjacent to the wall and in wakes due to the dissipation of vortex viscous flows. There is a higher level of entropy generation on the suction surface compared to the pressure surface. These losses can be seen in the upper half of the blade height as described in the previous sections. The separation at the pressure side is only limited to the middle of the blade toward the hub region. It should be noted that the relative velocity on the suction surface is higher than that on the pressure surface.

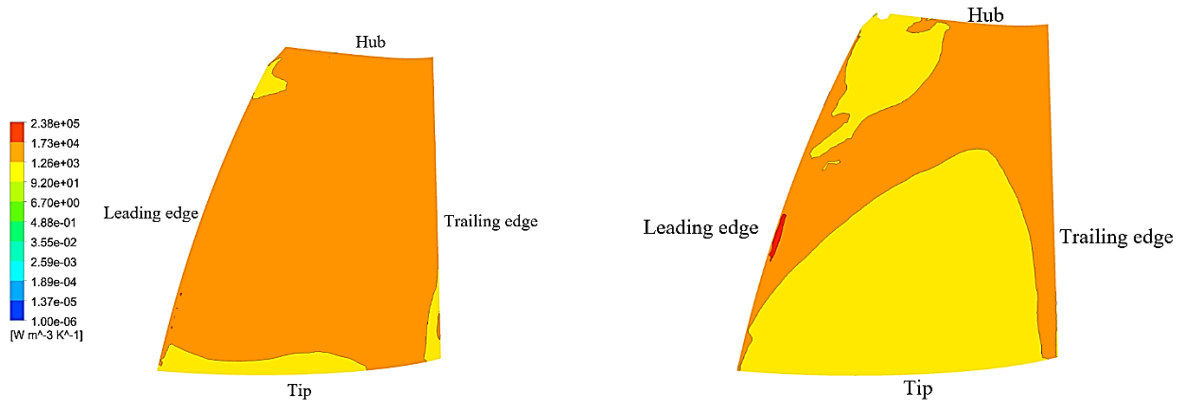

(a) Suction surface (b) Pressure surface

Fig. 11 Contours of total entropy generation on blade surface of CI impeller

Based on this analysis, design improvements of the selected irrigation pumps based on the findings can be investigated. At the inlet pipe, the PI design needs to modify thus reducing flow separation and entropy generation. The blade design has a tremendous effect on the energy losses of all impellers, especially at the leading edge and trailing edge near the hub and tip. The PI and TI design, the losses on the pressure surface are greater than those on the suction surface, except in the CI design. The design variables for improvement are including chord lengths, blade profile, blade span, blade angle, blade material, angle of attack, and angle of relative fluid velocity. These parameters can be used for further analysis.

5. CONCLUSION

A major cause of the lost efficiency in the surface water irrigation pump was investigated for further improvement. The entropy generation is applied to the pump on design improvement and loss sources' location and mechanisms. The CFD is used to analyze the design of pumps. First, the predicted entropy generation rate of each design is compared. Entropy generation is minimized at BEP. The results confirm clearly that CI is the highest efficiency pump with the lowest total entropy production rate, followed by TI and PI, respectively, as reported in Sanghirun and Asvapoositkul (2022). Second, the CFD results are concentrated in detailed flow fields as well as entropy generation of various designs to predict energy loss in areas such as the inlet section, impeller, or discharge pipe. Comparing the predicted entropy production on the blade surfaces with the flow field in all designs, we can conclude that the entropy production rate is high in the secondary flow direction and is consistent with free-stream velocity. The secondary flows are not a source of loss but simply move the loss.

Further analysis is possible in the entropy generation principle to be adopted to determine which features of the flow and entropy generation are relevant to the pump and attempt to develop a suitable improvement to gain an insight into the mechanism of the pump's response to entropy generation. For the design constraints (e.g. flow rate, head, and speed), the pump geometric parameters can be determined to obtain minimum levels of entropy generation. It is apparent that the relationship between traditional methods of design and irreversibility minimization techniques will be an integral part of engineering processes and components design. This will be further consideration of this project. Thus, entropy generation proves an excellent motivation to improve surface water irrigation pumps.

ACKNOWLEDGEMENTS

This research was supported by the Petchra Pra Jom Klao Ph.D. research Scholarship (Grant No. 48/2559), the Faculty of Engineering, the King Mongkut's University of Technology Thonburi (KMUTT), Project of Empowerment and Develop a New Generation of Researchers According to Research and Innovation Strategy (Graduate type) under National Research Council of Thailand (NRCT) in 2019 year, the Center of Excellence on Energy Technology and Environment (CEE), and the Ministry of Higher Education, Science, Research and Innovation (MHESI).

CONFLICTS OF INTERESTS

The authors declare that there is no conflict of interest regarding the publication of this paper.

AUTHORS CONTRIBUTION

Witthawat Sanghirun: Writing the original draft; Conceptualization; Methodology; Validation; Visualization; Funding acquisition. Wanchai Asvapoositkul: Supervision; review and editing.

REFERENCES

Ansys. (2018). *ANSYS CFX-Solver Theory Guide*.

Asvapoositkul, W., & Sanghirun, W. (2023). *A Conical Hollow-Shaped Impeller for Pump* (Thailand Patent No. 92384).

Barker, R., & Molle, F. (2004). *Evolution of irrigation in South and Southeast Asia* (Vol. 5). Iwmi.

Chinsuwan, W., & Cochran, B. (1985). Development and use of the axial flow lowlift pump in Thailand. KKU Enginering Journal. 12(2), 5-26.

Chinsuwan, W., & Cochran, B. (1986). *The axial-flow low-lift pump in Thailand*. Proceedings of International Conference on Small Farm Equipment for Developing Countries: Past Experiences and Future Priorities.

Denton, J. D. (1993). *Loss Mechanisms in Turbomachines*. https://doi.org/10.1115/93-GT-435

Gong, R., Wang, H., Chen, L., Li, D., Zhang, H., & Wei, X. (2013). Application of entropy production theory to hydro-turbine hydraulic analysis. *Science China Technological Sciences*, 56, 1636-1643. https://doi.org/10.1007/s11431-013-5229-y

Herwig, H., & Kock, F. (2007). Direct and indirect methods of calculating entropy generation rates in turbulent convective heat transfer problems. *Heat and mass transfer*, 43(3), 207-215. https://doi.org/https://doi.org/10.1007/s00231-006-0086-x

Hongyu, G., Wei, J., Yuchuan, W., Hui, T., Ting, L., & Diyi, C. (2021). Numerical simulation and experimental investigation on the influence of the clocking effect on the hydraulic performance of the centrifugal pump as turbine. *Renewable Energy*, 168, 21-30. https://doi.org/https://doi.org/10.1016/j.renene.2020.12.030

Huang, P., Appiah, D., Chen, K., Zhang, F., Cao, P., & Hong, Q. (2021). Energy dissipation mechanism of a centrifugal pump with entropy generation theory. *AIP Advances*, 11(4), 045208. https://doi.org/https://doi.org/10.1063/5.0042831

Ji, L., Li, W., Shi, W., Tian, F., & Agarwal, R. (2021). Effect of blade thickness on rotating stall of mixed-flow pump using entropy generation analysis. *Energy*, 236, 121381. https://doi.org/https://doi.org/10.1016/j.energy.2021.121381

Kock, F., & Herwig, H. (2004). Local entropy production in turbulent shear flows: a high-Reynolds number model with wall functions. *International Journal of Heat and Mass Transfer*, 47(10-11), 2205-2215. https://doi.org/https://doi.org/10.1016/j.ijheatmasstransfer.2003.11.025

Kock, F., & Herwig, H. (2005). Entropy production calculation for turbulent shear flows and their implementation in CFD codes. *International Journal of Heat and Fluid Flow*, 26(4), 672-680. https://doi.org/https://doi.org/10.1016/j.ijheatfluidflow.2005.03.005

Launder, B. E., & Spalding, D. B. (1974). The numerical computation of turbulent flows. *Journal of Computer Methods in Applied Mechanics and Engineering*, 3, 269-289. https://doi.org/https://doi.org/10.1016/0045-7825(74)90029-2

Li, D., Gong, R., Wang, H., Xiang, G., Wei, X., & Qin, D. (2016). Entropy production analysis for hump characteristics of a pump turbine model. *Chinese Journal of Mechanical Engineering*, 29, 803-812. https://doi.org/https://doi.org/10.3901/CJME.2016.0414.05

Mathieu, J., & Scott, J. (2000). *An introduction to turbulent flow*. Cambridge University Press. https://doi.org/https://doi:10.1017/CBO9781316529850

Natural Resources Conservation Service. (2016). *Chapter 8 irrigation pumping plants.* Part 623 irrigation national engineering handbook. Department of agriculture, United States.

Pei, J., Meng, F., Li, Y., Yuan, S., & Chen, J. (2016). Effects of distance between impeller and guide vane on losses in a low head pump by entropy production analysis. *Advances in Mechanical Engineering*, 8(11), 1687814016679568. https://doi.org/https://doi.org/10.1177/1687814016679568

Sanghirun, W., & Asvapoositkul, W. (2019). *Impeller*. (Thailand Patent No. 72934).

Sanghirun, W., & Asvapoositkul, W. (2020a). *Impeller for pump* (Thailand Patent No. 76916).

Sanghirun, W., & Asvapoositkul, W. (2020b). *Impeller for pump* (Thailand Patent No. 80214).

Sanghirun, W., & Asvapoositkul, W. (2022). Comparative design and performance of surface water irrigation pumps for smallholder farmers in South and Southeast Asia. *Journal of Mechanical Engineering and Sciences*, 16(3), 9025-9032. https://doi.org/https://doi.org/10.15282/jmes.16.3.2022.05.0714

Sciacovelli, A., Verda, V., & Sciubba, E. (2015). Entropy generation analysis as a design tool—A review. *Renewable and Sustainable Energy Reviews*, 43, 1167-1181. https://doi.org/https://doi.org/10.1016/j.rser.2014.11.104

Spurk, J. (1989). *Strömungslehre: Einführung in die Theorieder Strömungen* [Fluid mechanics: Introduction to the theory of fluid flows]. Springer-Verlag Berlin Heidellberg GmbH.

The Tham Luang Cave Rescue : A Global Mission. (2018). Report, Thailand.

Yang, F., Chang, P., Cai, Y., Lin, Z., Tang, F., & Lv, Y. (2022). Analysis of energy loss characteristics of vertical axial flow pump based on entropy production method under partial conditions. *Entropy*, 24(9), 1200. https://doi.org/https://doi.org/10.3390/e24091200

Yu, A., Tang, Y., Tang, Q., Cai, J., Zhao, L., & Ge, X. (2022). Energy analysis of Francis turbine for various mass flow rate conditions based on entropy production theory. *Renewable Energy*, 183, 447-458. https://doi.org/https://doi.org/10.1016/j.renene.2021.10.094.

Yu, S., & Colton, J. S. (2017, Aug. 21-25). Mixed-flow irrigation pump design optimization for Bangladesh. *The 21st International Conference on Engineering Design (ICED 17) Vancouver*, Canada.